



OPEN

GeSe ovonic threshold switch: the impact of functional layer thickness and device size

Jiayi Zhao^{1,2}, Zihao Zhao^{1,2}, Zhitang Song¹ & Min Zhu¹

Three-dimensional phase change memory (3D PCM), possessing fast-speed, high-density and nonvolatility, has been successfully commercialized as storage class memory. A complete PCM device is composed of a memory cell and an associated ovonic threshold switch (OTS) device, which effectively resolves the leakage current issue in the crossbar array. The OTS materials are chalcogenide glasses consisting of chalcogens such as Te, Se and S as central elements, represented by GeTe₆, GeSe and GeS. Among them, GeSe-based OTS materials are widely utilized in commercial 3D PCM, their scalability, however, has not been thoroughly investigated. Here, we explore the miniaturization of GeSe OTS selector, including functional layer thickness scalability and device size scalability. The threshold switching voltage of the GeSe OTS device almost lineally decreases with the thinning of the thickness, whereas it hardly changes with the device size. This indicates that the threshold switching behavior is triggered by the electric field, and the threshold switching field of the GeSe OTS selector is approximately 105 V/μm, regardless of the change in film thickness or device size. Systematically analyzing the threshold switching field of Ge–S and Ge–Te OTSs, we find that the threshold switching field of the OTS device is larger than 75 V/μm, significantly higher than PCM devices (8.1–56 V/μm), such as traditional Ge₂Sb₂Te₅, Ag–In–Sb–Te, etc. Moreover, the required electric field is highly correlated with the optical bandgap. Our findings not only serve to optimize GeSe-based OTS device, but also may pave the approach for exploring OTS materials in chalcogenide alloys.

Keywords Ovonic threshold switch, GeSe, Scalability, Selector, Threshold switching field, Phase change memory

With the development of information technology in the era of big data, storage devices play an increasingly important role. Currently, flash memory and dynamic random access memory (DRAM) dominate the semiconductor memory market, accounting for more than 97% of the market^{1,2}. However, high-density flash memory suffers from slow operation speed of approximately 100 μs and poor endurance of around 10⁴ cycles, while ultrafast DRAM consumes too much energy during each 65 ms refresh process³. To overcome these defects, new memory technologies have been developed, such as resistive random access memory (RRAM)^{4,5}, phase change memory (PCM)^{6,7}, magnetic random access memory (MRAM)^{8,9} and ferroelectric random access memory (FRAM)^{10,11}. Among these, PCM with a capacity of 128–256 Gb has been commercialized given its high density, fast speed and nonvolatile nature^{12,13}.

3D X-Point architecture, implemented in commercial 3D PCM, has been verified to be the best solution to achieve high-density storage, in which the key is the utilization of a two-terminal selector device known as ovonic threshold switch (OTS)^{14,15}. The OTS exhibits excellent selective performance, and its fabrication process is highly compatible with PCM. The requirements for OTS are strict, such as ≥ 10 mA/cm² working current, > 10⁴ selectivity (On-current/Off-current), as well as nanosecond switching speed^{16–18}. The OTS device has a sandwich structure, in which the middle layer is chalcogenide glass, called OTS material. Although hundreds of OTS materials have been found since first discovery in 1964¹⁹, the OTS materials cannot function without Te, Se and S chalcogens¹⁷, represented by GeTe₆^{18,20}, GeSe^{21–23} and GeS^{24,25}, respectively. Among them, As and Si co-doped GeSe OTS materials are believed to be the ones successfully utilized in commercial 3D PCM^{26,27}. However, the scalability of GeSe OTS still has not been thoroughly investigated, which inhibits the enhancement of storage capacity through device miniaturization^{28–30}. Therefore, in this work, the scalability characteristics in functional layer thickness and device size^{31–34} of traditional GeSe devices was investigated, which provides solutions for

¹State Key Laboratory of Functional Materials for Informatics, Shanghai Institute of Micro-System and Information Technology, Chinese Academy of Sciences, Shanghai 200050, China. ²University of Chinese Academy of Sciences, Beijing 100029, China. ✉email: minzhu@mail.sim.ac.cn

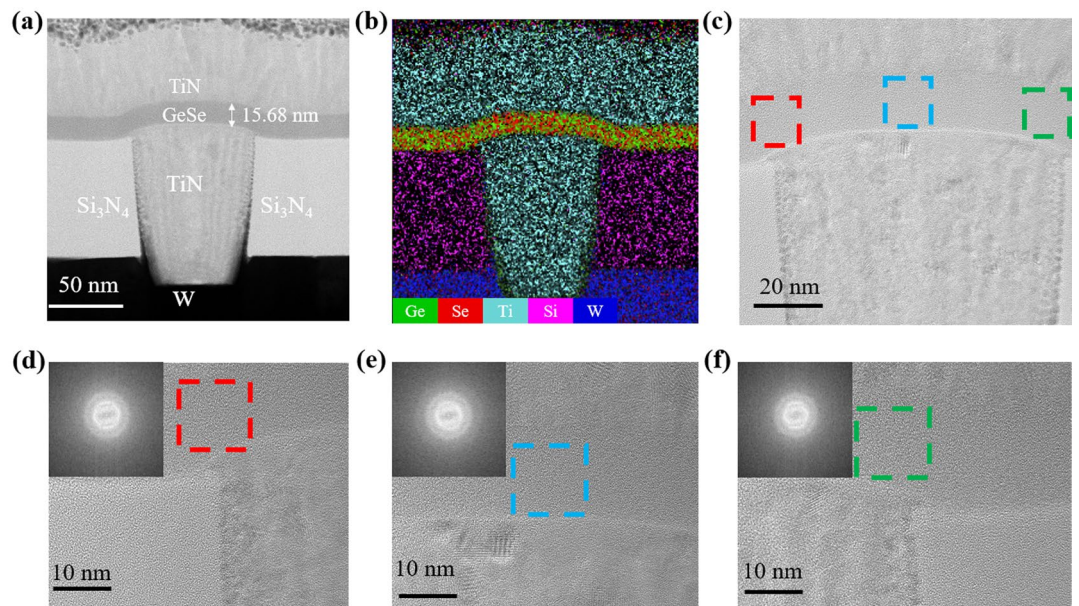


Figure 1. (a) Cross-sectional TEM of a GeSe device with a ~60 nm TiN plug. (b) EDS mapping of Ge, Se, Ti, N, Si and W. (c) Three different places of GeSe layer for local amplification. (d–f) HAADF-STEM image of GeSe layer at three locations, inset is the FFT image.

optimizing device's performance. Subsequently, the relationship between threshold switching field and optical bandgap was discovered, providing an effectively scheme for distinguishing OTS and PCM materials.

Experiment

We prepared GeSe T-shaped devices with different functional layer thicknesses and TiN-bottom electrode diameters. All the transition films were deposited by sputtering of GeSe target at room temperature, while the sputtering power of target was 20 W. The sputtering speed was measured through dividing thickness by time using scanning electron microscopy (SEM), which was ~1.45 nm/min. Besides, bottom TiN electrodes with different sizes were fabricated by 45 nm complementary metal oxide semiconductor (CMOS) technology. Finally, TiN was sputtered as top electrode. There were mainly two instruments used in studying the devices, which were Keithley 4200A-SCS parameter analyzer and MSO54 mixed signal oscilloscope. The former was for electrical performance, while the latter was used to capture the input pulses and device responses. The lamella used for transmission electron microscopy (TEM) investigation was prepared by focused ion beam (Helios, G4), which then was investigated by Cs-corrected TEM (JEOL, ARM 300).

Results and discussion

Figure 1a shows the cross-sectional TEM image of the T-shaped device with a ~15 nm-thick GeSe film³⁵. The ratio of Ge and Se elements in the film was approximately 54:46, which is close to 1:1. Next, the energy-dispersive spectroscopy (EDS) mappings were performed, including Ge, Se, Ti, Si and W elements, as shown in Fig. 1b. Different elements are homogeneously distributed without segregation or diffusion. To further investigate whether the GeSe film crystallized during fabrication process, the high angle annular dark field-scanning transmission electron microscopy (HAADF-STEM) images of GeSe film in three areas were observed. Figure 1d–f are local magnification of the corresponding positions in Fig. 1c in turn. The inset demonstrates fast Fourier transform (FFT) image. No obvious halo is observed around the bright spots in the center, indicating that the GeSe film is in an amorphous state.

Firstly, the scalability of functional layer thickness is studied through a series of electrical tests. Then, the current–voltage (I – V) behaviors of the GeSe device with all three functional layer thicknesses under 100 continuous triangular pulses were performed, as displayed in Fig. 2a. The electrode of all devices tested in this part is 200 nm. Taking 44 nm-thick GeSe device for instance, it suddenly transits to low resistance state between 4–5 V, which is called the threshold voltage (V_{th}). The fluctuation range of V_{th} is within 1 V, which is relatively small, demonstrating the device is stable and the results concerning scalability are reliable. After that, as the voltage decreases to 1–2 V, the device returns to the high resistance state, which is called the holding voltage (V_{hold}). Before normal switching, the device needs to be initialized by a stronger amplitude of voltage, which is called the fire voltage (V_{fire})^{36,37}. During the fire process, traps in the bandgap are rearranged, and thus the local state density change, which require more energy than normal switching circle³⁸. Figure 2b–d show the distribution of V_{th} and V_{hold} . V_{th} of devices with thickness of 44, 29 and 15 nm is roughly maintained at 3.8–4.8 V, 2.7–3.5 V and 1.5–2 V, respectively. Obviously, the V_{th} of the device almost lineally decreases as the GeSe layer thickness

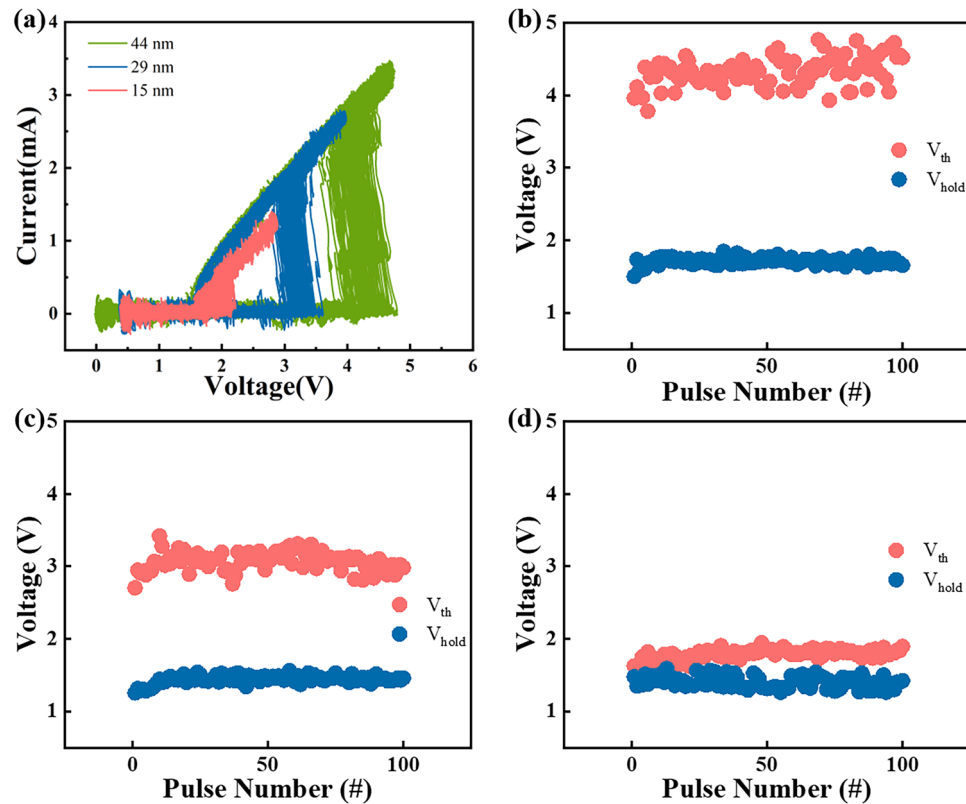


Figure 2. (a) I - V curves of different GeSe devices subjected to 100 consecutive triangular pulses after fire process. (b–d) Distribution of V_{th} and V_{hold} with different GeSe layer thicknesses of 44, 29 and 15 nm, respectively.

decreases. Meanwhile, the V_{hold} of the device with three different GeSe thicknesses is distributed between 1.1 and 1.7 V with minor decline.

It is also necessary to carry out experiments with different devices to increase the universality of the conclusion. As shown in Fig. 3a–c, four triangular pulses were applied to 20 different devices, including one fire pulse with higher voltage amplitude and three threshold pulses with smaller amplitude. The fire voltage of the device under the first pulse, as well as the threshold voltage and holding voltage of the device under the last pulse are counted. It could be seen that V_{fire} of 44, 29 and 15 nm thickness devices is distributed in 5.5–7 V, 5–5.5 V and 1.7–2.2 V with minor fluctuation. Combined with the previous conclusion, the V_{fire} and V_{th} of the device gradually increases with the increase of the thickness. Afterwards, Fig. 3d displays direct current (DC) I - V tests of GeSe device with different thicknesses and the leakage current at $1/2V_{th}$ is calculated. The leakage current, also known as I_{off} , plays a critical role in the storage array, which directly determines the power consumption of the whole chip and the integration density of the array^{18,39–41}. I_{off} is 2.4×10^{-8} , 4.94×10^{-8} and 2.54×10^{-8} A of 44, 29 and 15 nm thickness device, respectively. It's easy to observe the variation of switching voltage with different thicknesses, but the leakage current shows no obvious change.

As shown in Fig. 4a, the oscilloscope is used to capture the instantaneous responses of the device, enabling the measurement of the device's on and off-speed. An abrupt rise of current demonstrates the device is turned on and transits from a high resistance state to a low resistance state, while the time span represents the on-speed. Similarly, the time span of a sudden drop in current refers to the off-speed. In Fig. 4b, the on-speed of 44, 29 and 15 nm-thick devices are 8, 8 and 7 ns, while the off-speed of all three devices is 10 ns. To explore the transition mechanism of GeSe OTS selector, the threshold voltages and threshold switching field of different devices are calculated, where the electric field is obtained through dividing the threshold voltages calculated with 100 continuous pulses by the actual thickness of the film. Figure 4c illustrates the threshold voltage decreases linearly with the decrease of the GeSe layer thickness. In addition, the threshold switching field shows no significant change with the decrease of film thickness, maintaining a value around $105 \text{ V}/\mu\text{m}$ as shown in Fig. 4d.

Secondly, with the extension of Moore's law, the device gradually shrinks. As the device is three-dimensional, it's necessary to investigate its scalability characteristics in terms of both thickness and size. Therefore, exploring the scalability of the OTS device sizes is of great significance for the integration of 3D high-density storage arrays^{42,43}. In our work, as shown in Fig. 5, the GeSe layers are deposited on TiN bottom electrodes with diameters are 60, 120, 150 and 200 nm, respectively. Then, TiN is sputtered as the top electrode, at the bottom is the W interconnects, and TiN/GeSe/TiN layers are among them. An isolation layer is on both sides of the bottom electrode to isolate each cell.

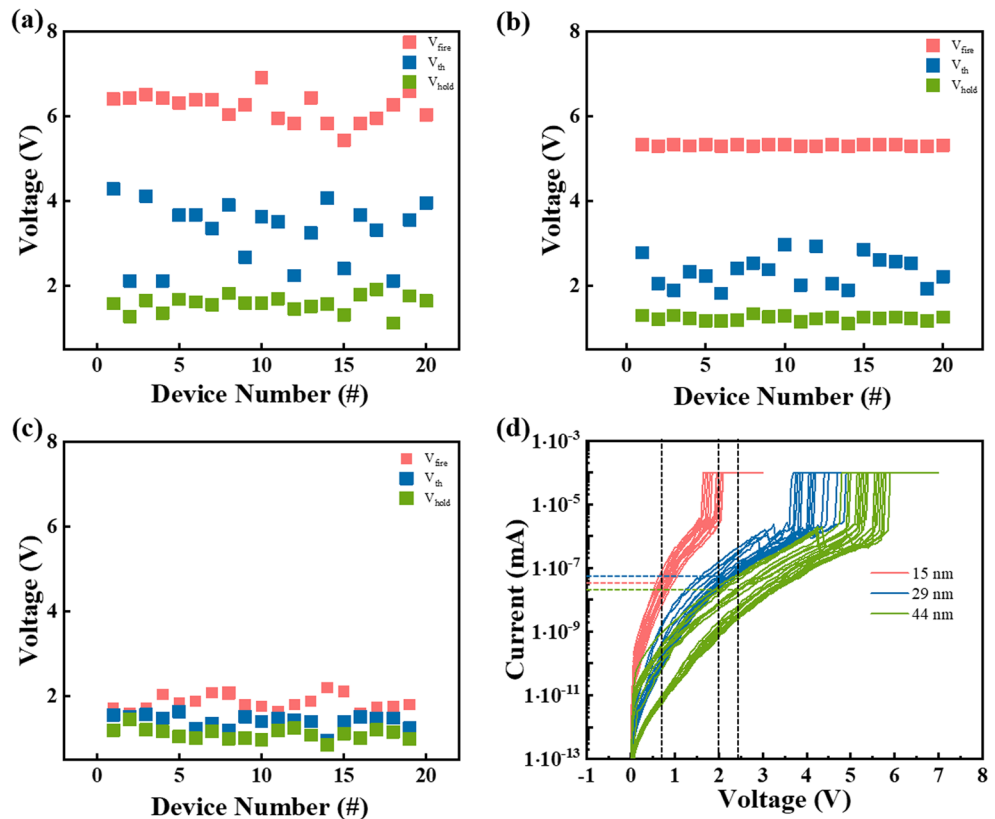


Figure 3. (a–c) Distribution of V_{fire} , V_{th} and V_{hold} with different GeSe layer thicknesses of 44, 29 and 15 nm, respectively. (d) DC I - V curves of GeSe devices in series with all three thicknesses.

The structure of arrays in the chip is composed of 2 bottom electrodes and 40 top electrodes, besides the cross structure on the left and right sides is for better alignment during lithography as shown in Fig. 6a. For electrical tests using Keithley 4200A-SCS parameter analyzer, two probes were pressed against the larger bottom electrode and the smaller top electrode. Triangular pulses were applied to devices with varying electrode sizes. From Fig. 6b, it is evident that V_{th} of devices with electrode sizes of 200, 150, 120 and 60 nm is distributed in 2–4 V. Moreover, the V_{th} does not vary significantly with changes in electrode size, indicating that V_{th} remains stable. Figure 6c–f display the specific distribution of V_{th} and V_{hold} , which is relatively concentrated and basically unchanged, demonstrating the high stability of the device. Meanwhile, the device with 60 nm electrode size shows wide discrete range of V_{th} , indicating the stability is worse than that of other devices with different electrode sizes, which needs to be improved by optimizing the manufacturing process.

Electrical tests were performed on 20 different devices at each electrode size, and the corresponding V_{fire} , V_{th} and V_{hold} were recorded, as shown in Fig. 7a–d. V_{fire} , V_{th} and V_{hold} of the four devices is 5–6 V, 1.5–3.5 V and 1–2 V with small fluctuations, showing the voltage distribution of the four devices is similar to each other. Figure 7e shows the DC I - V tests. I_{off} of the device with electrode size of 200, 150, 120 and 60 nm is 5.65×10^{-8} A, 4.59×10^{-8} A, 3.265×10^{-8} A and 2.35×10^{-8} A. That is, as the device size decreases, the leakage current also diminishes. Therefore, reducing the electrode size of the device is a helpful way to improve the storage density of the array. At last, the switching speed is measured, and Fig. 7f displays the comparison of various devices. The on-speed of GeSe device with electrode size of 200, 150, 120 and 60 nm is 8, 10, 10 and 9 ns, while the off-speed is 10, 10, 9 and 9 ns, respectively. Compared with Fig. 4b, both the on-speed and off-speed are distributed between 7 and 10 ns for all devices. Not only is the speed of the device measured manually with an error range of 1–2 ns, but there is also no order of magnitude difference. Therefore, the subtle difference could be ignored, and the switching speed is not related to the device variability.

Figure 8a displays the V_{th} and threshold switching field of GeSe devices with different electrode sizes. Obviously, although the device size changes, V_{th} and electric field distribution are basically along a horizontal line. Specifically, V_{th} and the threshold switching field are distributed at around 3 V and 105 V/ μm , respectively. Typically, V_{th} is used to describe the critical point at which OTS and PCM change from high resistance to low resistance. However, due to the different thicknesses of functional layer, V_{th} can change greatly. Therefore, the average threshold switching field of common OTS and PCM devices is statistically analyzed, effectively avoiding the influence of the functional layer's thickness, as shown in Fig. 8b. Moreover, in Fig. 8c, the detail data of the materials investigated is listed. Three OTS materials, GeTe₆, GeSe and GeS, exhibit electric field ranging from 75 to 175 V/ μm^{24} . In addition, the average threshold switching field of six PCM materials, Ge₁₅Sb₈₅, Ti-Sb-Te (TST), Ag-In-Sb-Te (AIST), Sc-Sb-Te (SST), Sb and Ge₂Sb₂Te₅ (GST), is distributed in 8.1–56 V/ $\mu\text{m}^{33,44-48}$. Threshold

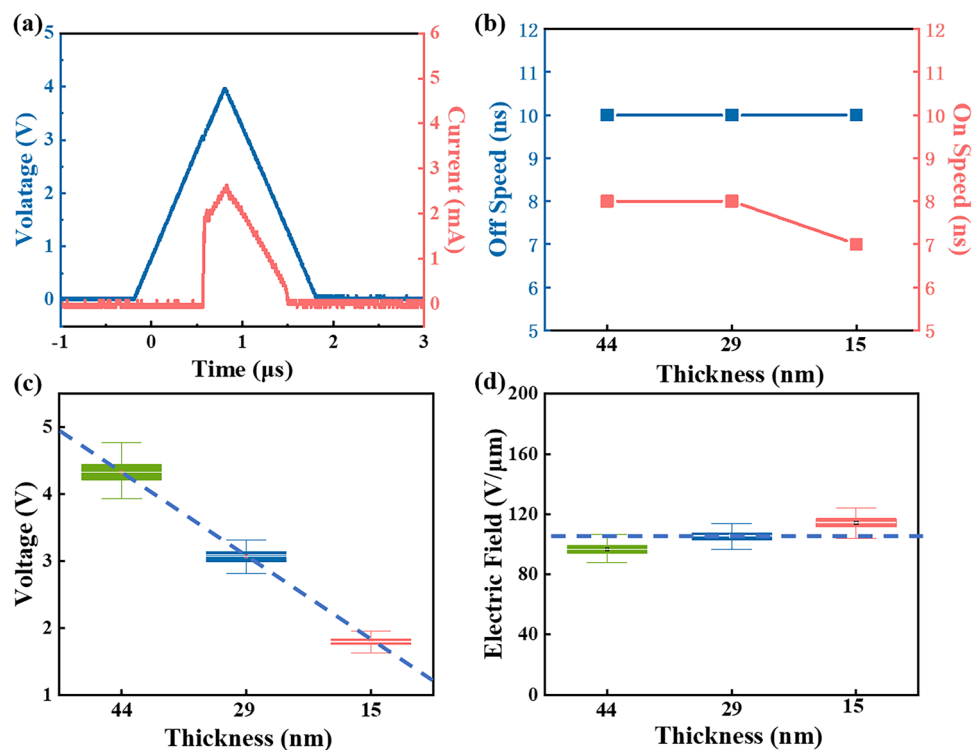


Figure 4. (a) Triangular pulse and corresponding curve when measuring device's speed. (b) Statistical switching speeds distribution of various GeSe devices. (c) Relationship between threshold voltage of GeSe device and thickness of transition layer. (d) Relationship between threshold switching field of GeSe device and transition layer thickness.

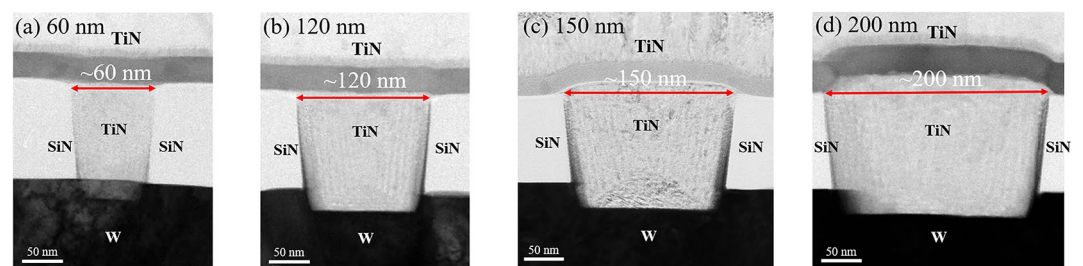


Figure 5. Cross-sectional TEM images of GeSe devices with ~ 60, 120, 150 and 200 nm TiN plug, respectively.

voltage increases with the broaden of bandgap, regardless of traps²⁵. Thus, for different kinds of devices with same thickness, the one with wider bandgap exhibits larger threshold transition field. Noticeably, the electric field of OTS is above 70 V/μm, significantly larger than that of PCM (< 60 V/μm). However, regardless of OTS or PCM, the electric field is approximately linear with the optical bandgap. Besides, the OTS materials typically possess a bandgap greater than that of PCM materials. This characteristic may be utilized as a criterion for screening potential OTS materials candidates in chalcogenides.

Conclusions

In this paper, the scalability characteristics of traditional GeSe OTS selector are comprehensively investigated, including functional layer thickness scalability and electrode size scalability. On one hand, when the thickness of the functional layer is reduced from 44 to 15 nm, V_{fire} , V_{th} and V_{hold} decreases from 7 to 2.2 V, 4.8 to 2 V and 1.8 V to 1.2 V, respectively. Besides, I_{off} is basically maintained at 30 nA and the electric field remained around 105 V/μm, both of which don't change with the variation of the thickness. On the other hand, as the device size decreases from 200 to 60 nm, V_{fire} , V_{th} , V_{hold} and electric field is distributed at 5–6 V, 1.5–3.5 V, 1–2 V and around

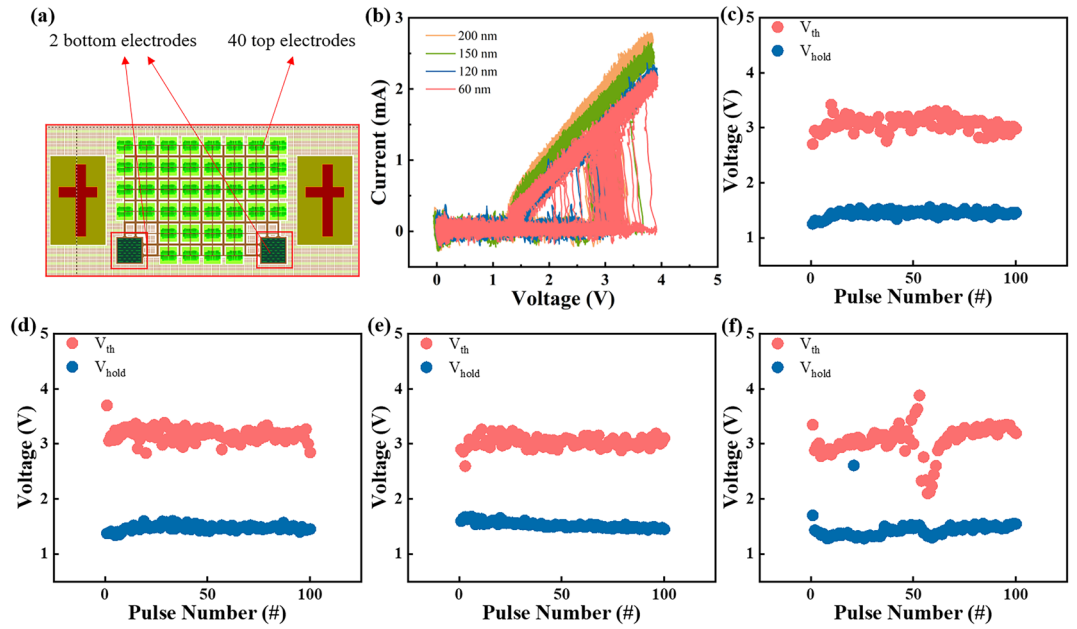


Figure 6. (a) Structure of arrays in the chip. (b) I - V curves of different GeSe devices subjected to 100 consecutive triangular pulses after fire process. (c-f) Distribution of V_{th} and V_{hold} with different electrode sizes of 200, 150, 120 and 60 nm, respectively.

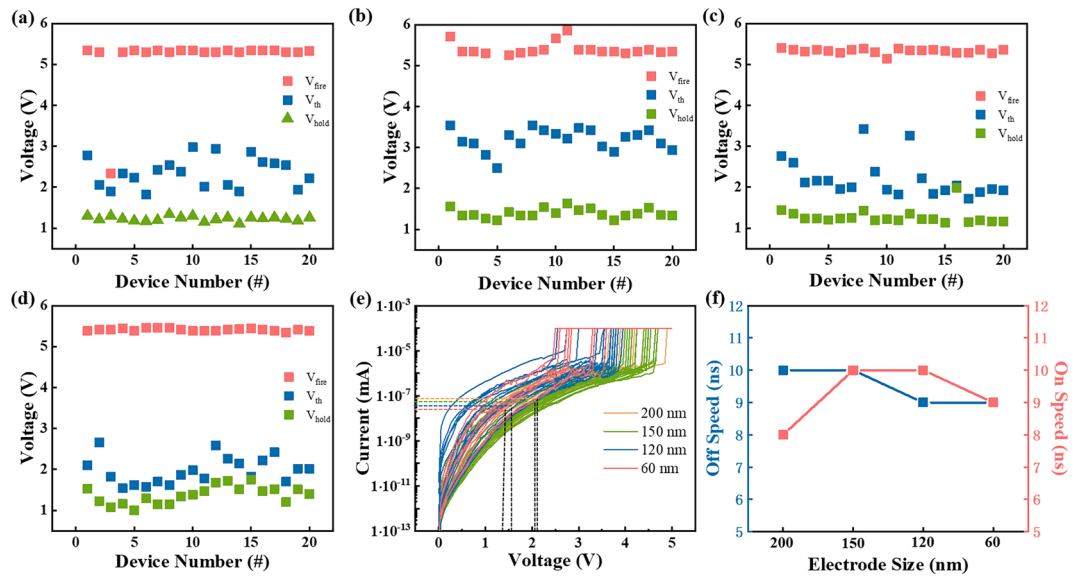


Figure 7. (a-d) Distribution of V_{fire} , V_{th} and V_{hold} with different electrode sizes of 200, 150, 120 and 60 nm, respectively. (e) DC I - V curves of GeSe devices in series with all four electrode sizes. (f) Statistical switching speeds distribution of various GeSe devices.

105 V/ μ m, remaining unchanged on the whole. At the same time, I_{off} decreases from 56.5 to 23.5 nA. In summary, the electric field of GeSe OTS selector is basically unchanged regardless of thickness or size reduction, indicating an electric field-driven switching mechanism. Meanwhile, the leakage current decreases with the reduction of the device size, and the switching voltage decreases with the reduction of the thickness, reflecting its great potential in large-scale high-density memory. To sum up, the 15 nm thick device with the electrode size of 60 nm demonstrates the best performance. Finally, it is concluded that the threshold switching field increases linearly with the increase of optical bandgap. The OTS materials typically possess a bandgap larger than PCM materials. This characteristic may be utilized as a criterion for screening potential OTS material candidates in chalcogenides.

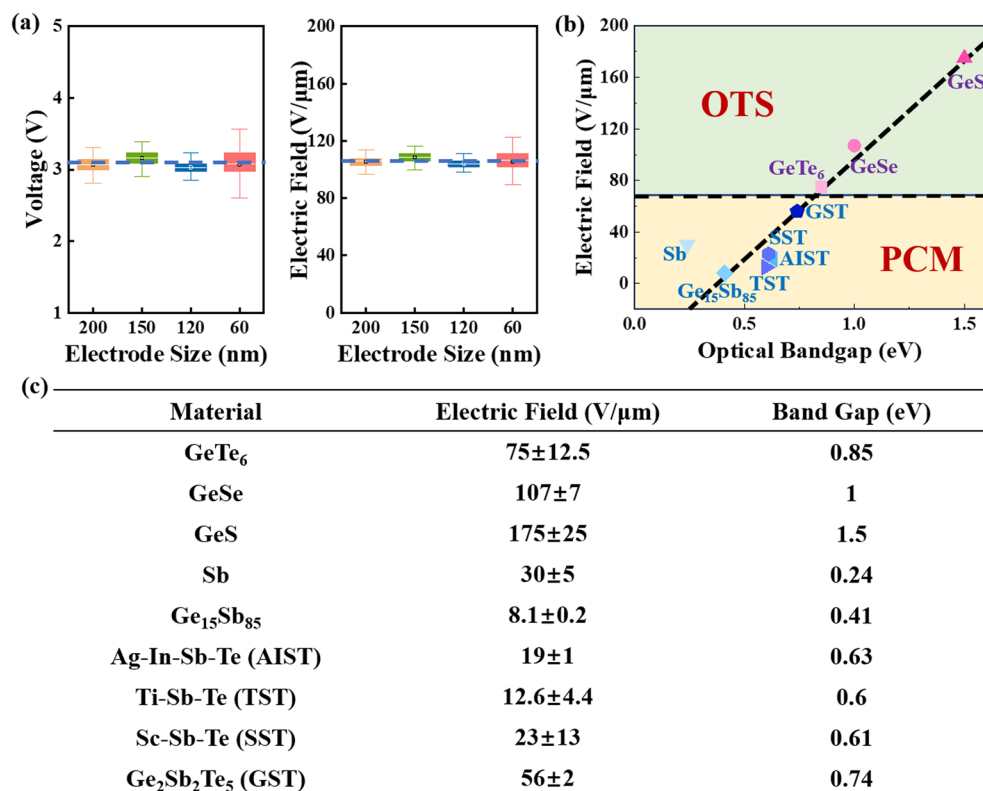


Figure 8. (a) The tendency of GeSe device's threshold voltage and electric field with electrode size changing. (b) Intuitive comparison on the relationship between electric field and optical bandgap of common OTS and PCM materials. (c) Electric field and optical bandgap values of common OTS and PCM materials.

Data availability

The data that support the findings of this study are available from the corresponding author upon reasonable request.

Received: 19 December 2023; Accepted: 12 March 2024

Published online: 20 March 2024

References

- Wong, H. S. P. & Salahuddin, S. Memory leads the way to better computing. *Nat. Nanotechnol.* **10**, 191–194 (2015).
- Hwang, C. S. Prospective of semiconductor memory devices: From memory system to materials. *Adv. Electron. Mater.* **1**, 1400056 (2015).
- Kim, B. K. & Lee, D. H. LSF: A new buffer replacement scheme for flash memory-based portable media players. *IEEE Trans. Consum. Electron.* **59**, 130–135 (2013).
- Waser, R., Dittmann, R., Staikov, C. & Szot, K. Redox-based resistive switching memories nanoionic mechanisms, prospects, and challenges. *Adv. Mater.* **21**, 2632–2663 (2009).
- Wu, H. *et al.* Resistive random access memory for future information processing system. *Proc. IEEE* **105**, 1770–1789 (2017).
- Wuttig, M. Phase-change materials: Towards a universal memory? *Nat. Mater.* **4**, 265–266 (2005).
- Atwood, G. Phase-change materials for electronic memories. *Science* **321**, 210–211 (2008).
- Nishimura, N. *et al.* Magnetic tunnel junction device with perpendicular magnetization films for high-density magnetic random access memory. *J. Appl. Phys.* **91**, 5246–5249 (2002).
- Girard, P. *et al.* A survey of test and reliability solutions for magnetic random access memories. *Proc. IEEE* **109**, 149–169 (2021).
- Bosser, A. L. *et al.* Single-event effects in the peripheral circuitry of a commercial ferroelectric random access memory. *IEEE Trans. Nucl. Sci.* **65**, 1708–1714 (2018).
- Mikolajick, T., Slesazek, S., Park, M. H. & Schroeder, U. Ferroelectric hafnium oxide for ferroelectric random-access memories and ferroelectric field-effect transistors. *MRS Bull.* **43**, 340–346 (2018).
- Burr, G. W. *et al.* Large-scale (512 kbit) integration of multilayer-ready access-devices based on mixed-ionic-electronic-conduction (MIEC) at 100% yield. In *Dig. Tech. Pap. Symp. VLSI Technol.* 41–42. <https://doi.org/10.1109/VLSIT.2012.6242451> (2012).
- Shen, J. *et al.* Toward the speed limit of phase-change memory. *Adv. Mater.* **35**, 2208065 (2023).
- Cho, B. *et al.* Rewritable switching of one diode-one resistor nonvolatile organic memory devices. *Adv. Mater.* **22**, 1228–1232 (2010).
- Park, J., Yoo, J., Song, J., Sung, C. & Hwang, H. Hybrid selector with excellent selectivity and fast switching speed for X-point memory array. *IEEE Electron Device Lett.* **39**, 1171–1174 (2018).
- Zhu, M., Ren, K. & Song, Z. Ovonic threshold switching selectors for three-dimensional stackable phase-change memory. *MRS Bull.* **44**, 715–720 (2019).
- Zhao, Z. *et al.* Chalcogenide ovonic threshold switching selector. *Nano-Micro Lett.* **16**, 1–40 (2024).
- Velea, A. *et al.* Te-based chalcogenide materials for selector applications. *Sci. Rep.* **7**, 8103 (2017).

19. Ovshinsky, S. R. Reversible electrical switching phenomena in disordered structures. *Phys. Rev. Lett.* **21**, 1450–1453 (1968).
20. Anbarasu, M., Wimmer, M., Bruns, G., Salinga, M. & Wuttig, M. Nanosecond threshold switching of GeTe₂ cells and their potential as selector devices. *Appl. Phys. Lett.* **100**, 743 (2012).
21. Clima, S. *et al.* Ovonic threshold-switching Ge_xSe_{1-x} chalcogenide materials: Stoichiometry, trap nature, and material relaxation from first principles. *Phys. Status Solidi Rapid Res. Lett.* **14**, 1900672 (2020).
22. Kim, S. D. *et al.* Effect of Ge concentration in Ge_xSe_{1-x} chalcogenide glass on the electronic structures and the characteristics of ovonic threshold switching (OTS) devices. *ECS Solid State Lett.* **2**, 75 (2013).
23. Govoreanu, B. *et al.* Thermally stable integrated Se-based OTS selectors with >20 MA/cm² current drive, >3.10³ half-bias non-linearity, tunable threshold voltage and excellent endurance. In *Dig. Tech. Pap. Symp. VLSI Technol.* T92–T93. <https://doi.org/10.23919/VLSIT.2017.7998207>. (2017).
24. Jia, S., Li, H., Liu, Q., Song, Z. & Zhu, M. Scalability of sulfur-based ovonic threshold selectors for 3D stackable memory applications. *Phys. Status Solidi Rapid Res. Lett.* **15**, 2100084 (2021).
25. Jia, S. *et al.* Ultrahigh drive current and large selectivity in GeS selector. *Nat. Commun.* **11**, 4636 (2020).
26. Wu, R. *et al.* The role of arsenic in the operation of sulfur-based electrical threshold switches. *Nat. Commun.* **14**, 6095 (2023).
27. Choe, J. Memory technology 2021: Trends challenges. In *Int. Conf. Simul. Semicond. Process. Devices, SISPAD 2021-September*, 111–115 (2021).
28. Alimkhanuly, B., Kim, S., Kim, L. W. & Lee, S. Electromagnetic analysis of vertical resistive memory with a sub-nm thick electrode. *Nanomaterials* **10**, 1634 (2020).
29. Chen, H. Y. *et al.* Experimental study of plane electrode thickness scaling for 3D vertical resistive random access memory. *Nanotechnology* **24**, 465201 (2013).
30. Ahn, H. W. *et al.* A study on the scalability of a selector device using threshold switching in Pt/GeSe/Pt. *ECS Solid State Lett.* **2**, 31–34 (2013).
31. Liu, G. *et al.* The investigations of characteristics of GeSe thin films and selector devices for phase change memory. *J. Alloys Compd.* **792**, 510–518 (2019).
32. Li, H. & Chen, W. First-principles prediction of the native filament: Dielectric interfaces for the possible filamentary switching mechanism in chalcogenide selector devices. *J. Appl. Phys.* **127**, 916 (2020).
33. Shportko, K. *et al.* Resonant bonding in crystalline phase-change materials. *Nat. Mater.* **7**, 653–658 (2008).
34. Ren, K. *et al.* Electrical switching properties and structural characteristics of GeSe–GeTe films. *Nanoscale* **11**, 1595–1603 (2019).
35. Nam, S. W. *et al.* Electrical wind force-driven and dislocation-templated amorphization in phase-change nanowires. *Science* **336**, 1561–1566 (2012).
36. Butcher, B. *et al.* Hot forming to improve memory window and uniformity of low-power HfO_x-based RRAMs. In *2012 4th IEEE Int. Mem. Work. IMW 2012* 1–4. <https://doi.org/10.1109/IMW.2012.6213647> (2012).
37. Kim, T., Lee, D., Kim, J. & Sohn, H. Firing voltage reduction in thermally annealed Ge–As–Te thin film with ovonic threshold switching. *J. Vac. Sci. Technol. B Nanotechnol. Microelectron. Mater. Process. Meas. Phenom.* **38**, 36 (2020).
38. Avasarala, N. S. *et al.* Doped GeSe materials for selector applications. In *Eur. Solid-State Device Res. Conf.* 168–171. <https://doi.org/10.1109/ESSDERC.2017.8066618> (2017).
39. Cheng, H. Y. *et al.* Ultra-high endurance and low I_{OFF} selector based on AsSeGe chalcogenides for wide memory window 3D stackable crosspoint memory. In *Tech. Dig. Int. Electron Devices Meet. IEDM 2018-December*, 1–4 (2018).
40. Li, X., Yuan, Z., Lv, S., Song, S. & Song, Z. Extended endurance performance and reduced threshold voltage by doping Si in GeSe-based ovonic threshold switching selectors. *Thin Solid Films* **734**, 138837 (2021).
41. Koo, Y., Lee, S., Park, S., Yang, M. & Hwang, H. Simple binary ovonic threshold switching material SiTe and its excellent selector performance for high-density memory array application. *IEEE Electron Device Lett.* **38**, 568–571 (2017).
42. Gopalakrishnan, K. *et al.* Highly scalable novel access device based on mixed ionic electronic conduction (MIEC) materials for high density phase change memory (PCM) arrays. In *Dig. Tech. Pap. Symp. VLSI Technol.* Vol. 1, 205–206 (2010).
43. Salahuddin, S., Ni, K. & Datta, S. The era of hyper-scaling in electronics. *Nat. Electron.* **1**, 442–450 (2018).
44. Luckas, J. *et al.* Defects in amorphous phase-change materials. *J. Mater. Res.* **28**, 1139–1147 (2013).
45. Krebs, D. *et al.* Threshold field of phase change memory materials measured using phase change bridge devices. *Appl. Phys. Lett.* **95**, 8 (2009).
46. Zhu, M. *et al.* The micro-structure and composition evolution of Ti–Sb–Te alloy during reversible phase transition in phase change memory. *Appl. Phys. Lett.* **104**, 560 (2014).
47. Rao, F. *et al.* Reducing the stochasticity of crystal nucleation to enable subnanosecond memory writing. *Science* **358**, 1423–1427 (2017).
48. Kato, T. & Tanaka, K. Electronic properties of amorphous and crystalline Ge₂Sb₂Te₅ films. *Jpn. J. Appl. Phys.* **44**, 7340 (2005).

Acknowledgements

Financial support was provided by the Strategic Priority Research Program of the Chinese Academy of Sciences (XDB44010200). M. Zhu acknowledges support by the National Outstanding Youth Program (62322411), Hundred Talents Program (Chinese Academy of Sciences) and the Shanghai Rising-Star Program (21QA1410800).

Author contributions

J. Z. and Z. Z. deposited the film, prepared the devices and measured device performances. J. Z. and M. Z. wrote the paper. Z. S. discussed the results and commented on the manuscript. The project was initiated and conceptualized by M. Z.

Competing interests

The authors declare no competing interests.

Additional information

Correspondence and requests for materials should be addressed to M.Z.

Reprints and permissions information is available at www.nature.com/reprints.

Publisher's note Springer Nature remains neutral with regard to jurisdictional claims in published maps and institutional affiliations.



Open Access This article is licensed under a Creative Commons Attribution 4.0 International License, which permits use, sharing, adaptation, distribution and reproduction in any medium or format, as long as you give appropriate credit to the original author(s) and the source, provide a link to the Creative Commons licence, and indicate if changes were made. The images or other third party material in this article are included in the article's Creative Commons licence, unless indicated otherwise in a credit line to the material. If material is not included in the article's Creative Commons licence and your intended use is not permitted by statutory regulation or exceeds the permitted use, you will need to obtain permission directly from the copyright holder. To view a copy of this licence, visit <http://creativecommons.org/licenses/by/4.0/>.

© The Author(s) 2024